Geomechanics and Engineering, *Vol. 35*, *No. 1 (2023) 13-27*
https://doi.org/10.12989/gae.2023.35.1.013

Analytical study on seepage behavior of a small-scale capillary barrier system under lateral no-flow condition

Byeong-Su Kim*

Department of Civil & Environmental Engineering, Dankook University,
152, Jukjeon-ro, Suji-gu, Yongin City, Gyeonggi-do 16890, Korea

(*Received June 11, 2022, Revised August 15, 2022, Accepted August 16, 2022*)

Abstract. The model production for large-scale (lateral length ≥ 2.0 m) capillary barrier (CB) model tests is time and cost-intensive. To address these limitations, the framework of a small-scale CB (SSCB) model test under the lateral no-flow condition has been established. In this study, to validate the experimental methodology of the SSCB model test, a series of seepage analyses on the SSCB model test and engineered slopes in the same and additional test conditions was performed. First, the seepage behavior and diversion length (L_D) of the CB system were investigated under three rainfall conditions. In the seepage analysis for the engineered slopes with different slope angles and sand layer thicknesses, the L_D increased with the increase in the slope angle and sand layer thickness, although the increase rate of the L_D with the sand layer thickness exhibited an upper limit. The L_D values from the seepage analysis agreed well with the results estimated from the laboratory SSCB mode test. Therefore, it can be concluded that the experimental methodology of the SSCB model test is one of the promising alternatives to efficiently evaluate the water-shielding performance of the CB system for an engineered slope.

Keywords: CB model test; diversion length; lateral no-flow condition; seepage analysis; small-scale capillary barrier

1. Introduction

To increase the stability of the geo-structures (e.g., levees, embankments, road slopes, and landfills) against rainwater infiltration, it is important to prevent or mitigate the infiltration of water in unsaturated soil in layered slopes (Miyazaki 1988, Rahardjo *et al*. 2011, Kim and Jeong 2017, Deng *et al*. 2019, Satyanaga *et al*. 2022). One of the representative tools to prevent such infiltration is the capillary barrier (CB) system (Ross 1990). The CB system has a simple geo-structure in which a layer of large-grained gravel is placed on a sand layer (Khire *et al.* 2000, Walter *et al*. 2000, Li *et al*. 2021). Owing to the different water retention characteristics of the two soil layers, CB systems can prevent the infiltration of water into the sand layer and appropriately direct the infiltrated water flow between the two layers (Ross 1990, Kung 1990, Steenhuis *et al*. 1991).

In other words, the CB system exhibits water-shielding capabilities. Moreover, because CB systems typically consist of eco-friendly geomaterials such as sand and gravel, they are characterized by a long service life, simple construction, and low cost (Ross 1990, Benson and Khire 1995). Consequently, such systems have been widely used to prepare geo-structures for various purposes, such as landfill cover systems for waste disposal sites, oxygen barriers to limit acid mine drainage, closures for nuclear waste facilities, and water-shielding protection systems for engineered slopes (ex., Hill and Parlange 1972, Rasmuson and Eriksson 1986, Nicholson *et al*. 1989, Morel-Seytoux 1993, Kämpf and Montenegro 1997, Bussière *et al*. 2003, Parent and Cabral *et al*. 2006, Mancarella *et al.* 2012, Hey and Simms 2021).

Many experimental and numerical studies have been conducted to evaluate and enhance CB systems for the stability of the geo-structure (ex., Oldenburg 1993, Morris and Stormont *et al*. 1998, Mohamed *et al*. 1997, Bussière *et al*. 2002, Tami *et al*. 2004, Aubertin *et al*. 2009, Ng *et al*. 2014, Zhan *et al*. 2014, Matsumoto *et al*. 2016, Tang *et al*. 2020, Li *et al.* 2021). Most of the models in experimental studies involving laboratory CB model tests have a length of more than 2.0 m. The use of a large-scale model with a lateral length ≥ 2.0 m renders it difficult to perform experiments in various conditions and enhances the water-shielding performance of the CB system. Thus, it is required to propose an improved experimental methodology to replace such a large- scale model test.

Kim (2021) proposed a small-scale CB (SSCB) model test framework to decrease the time and cost associated with the large-scale CB model, as shown in Fig. 1. In particular, it should be noted that the drainage condition of the flow direction of the inclined sand layer in SSCB model tests was set as the lateral no-flow condition to ensure rapid infiltration into the gravel layer. A series of SSCB model tests under three rainfall intensities (20, 50, and 100 mm/h) was performed. To evaluate the effectiveness of the SSCB model test, the diversion lengths (L_D) representing the water-shielding performance of the CB system were estimated using an empirical equation for the lateral flow condition based on the physical and water retention characteristics of sand and gravel, and the results were compared to those obtained using the SSCB model test. The

*Corresponding author, Associate Professor
E-mail: bs.kim@dankook.ac.kr

Copyright © 2023 Techno-Press, Ltd.

ISSN: 2005-307X (Print), 2092-6219 (Online)

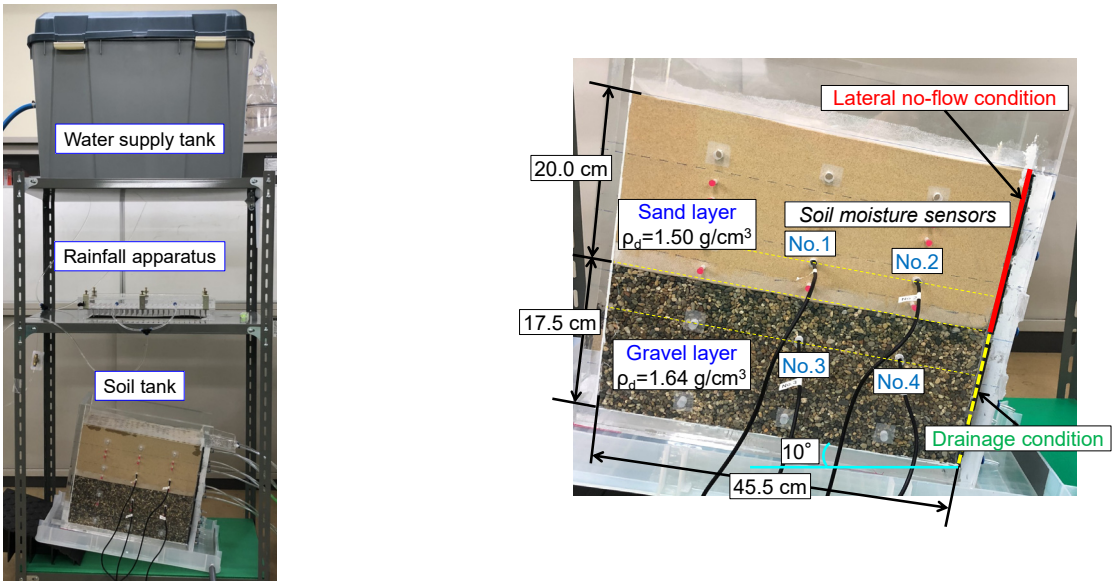

(a) Apparatus of the SSCB model test (b) Setting condition

Fig. 1 Apparatus and setting conditions for the laboratory SSCB model test (After Kim *et al*. 2021)

SSCB model corresponded to a smaller testing time and reduced production work to evaluate the water-shielding performance of the CB system.

In this study, to verify the validity of the experimental methodology of the SSCB test performed by Kim (2021) for the CB system, two seepage analyzes were performed. First, a series of seepage analyses on the SSCB model test under the same conditions were carried out. The infiltration behavior and L_D values of the CB system were investigated under three rainfall intensities (I = 20, 50, and 100 mm/h), and compared to the results of the SSCB model test. Next, to efficiently evaluate the water-shielding performance of the CB system for an engineered slope, a series of seepage analyses on the engineered slopes were performed under I = 20 mm/h for 24 h at different slope angles (i.e., 1:1.5, 1:2.5, and 1:6.0) and sand layer thickness values (i.e., 20, 40, and 60 cm). The effects of the slope angle and sand layer thickness on L_D were investigated. The L_D values estimated from the seepage analysis for the engineered slope under the same conditions as the SSCB model test were compared with those of the model test. Based on the obtained results, the experimental methodology of the SSCB model test with the water-shielding performance of the CB system for an engineered slope was discussed.

2. Numerical analysis of CB system for laboratory SSCB model test

A numerical analysis assuming the lateral no-flow (i.e., undrained) condition of the sand layer, as in the SSCB model test performed by Kim (2021) as shown in Fig. 1, is conducted to investigate the change in the infiltration behavior and diversion length of the CB system in a rainfall event. To evaluate the efficiency of the SSCB model for designing a CB system, the obtained analysis results are compared with those of the SSCB model test.

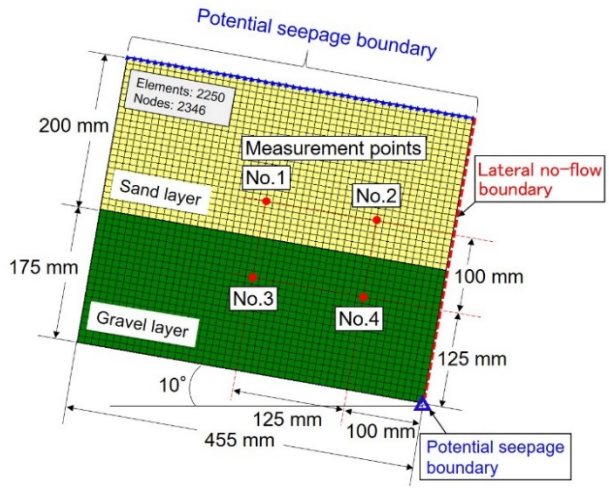

Fig. 2 Modeling of seepage analysis on the setting condition of the laboratory SSCB model test

2.1 Modelling

The seepage analysis in this study was performed using the finite element method using SEEP/W (2004) program to evaluate the infiltration behavior in the laboratory CB model test. As in the laboratory CB model test, as shown in Fig. 1(b), the analysis model was set to have a sand layer with a width and height of 455 and 200 mm, respectively, and a gravel layer with a width and height of 455 mm and 175 mm, respectively, as shown in Fig. 2. The slope angle was set as 10°. The number of elements and nodes in the analysis model were 2250 and 2346, respectively, to ensure that the seepage analysis model could measure the L_D. In the laboratory CB model test performed by Kim (2021), four soil moisture sensors (EC-5, Decagon Devices Co.) were installed inside the soil tank to measure the variations in the volumetric water content (VWC) due to water infiltration. The size of the soil moisture sensor (EC-5) is

Table 1 Physical properties of the soil samples

Sample	Toyoura sand	Silica sand No.1	Masado
G_s (g/cm^3)	2.64	2.65	2.58
w_L (%)	-	-	24.6
w_p (%)	-	-	N.P
$\rho_{d\,max}$ (g/cm^3)	1.64	1.67	1.88
$\rho_{d\,min}$ (g/cm^3)	1.37	1.45	-
D_{50} (cm)	1.69	4.65	0.38
F_c (%)	0	0	18.4
C_u	1.63	2.24	13.7
C_c	0.97	0.84	
k_{sat} (m/s)	1.45×10^{-4}	2.44×10^{-3}	1.40×10^{-6}

Note: G_s = specific gravity, w_L = liquid limit, w_p = plastic limit, $\rho_{d\,max}$ & $\rho_{d\,min}$ = maximum and minimum dry densities, D_{50} = mean particle size, F_c = passing percent under 75μm, C_u = uniformity coefficient, C_u = curvature coefficient, and k_{sat} = saturated hydraulic conductivity

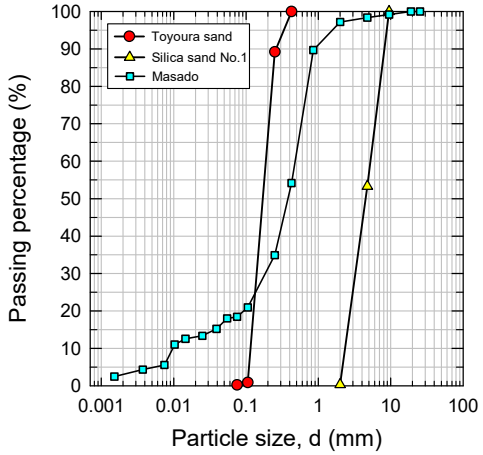

Fig. 3 Grain size distribution curves of the soil samples

8.9 × 1.8 × 0.7 cm (length × width × thickness), and it has parts of an electronic circuit (length: 3.4 cm) and two probes (length: 5.5 cm). This sensor can measure the VWC from 0 to 100% and has a measuring capacity of 240 ml.

Since the precision is ±1~2% of the VWC, it is possible to measure the volumetric moisture content with very high precision. The measurement time is 10 ms (= 0.01 s). The VWC variations in the seepage analysis were measured considering the same installation locations of the soil moisture sensors as those in the model test, as shown in Fig. 2.

2.2 Input parameters and analysis condition

In the SSCB model test performed by Kim (2021), Toyoura sand and silica sand No. 1 were used as materials for sand and gravel layers, respectively. Fig. 3 shows the particle size distribution of three soils including decomposed granite soil (i.e., Masado) applied as the soil of the overlayer in the seepage analysis for the CB system of the engineered slope described later. The physical properties with hydraulic conductivities of the soil samples are summarized in Table 1. Notably, since the saturation permeability coefficients of Toyoura sand and silica sand

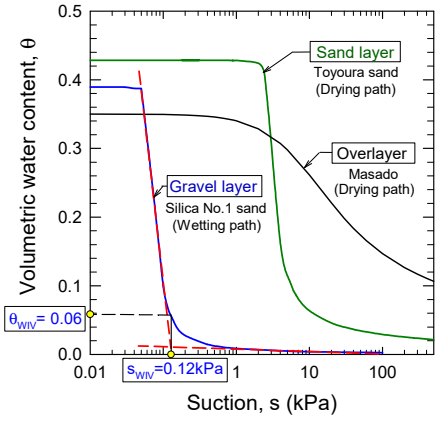

(a) SWCC

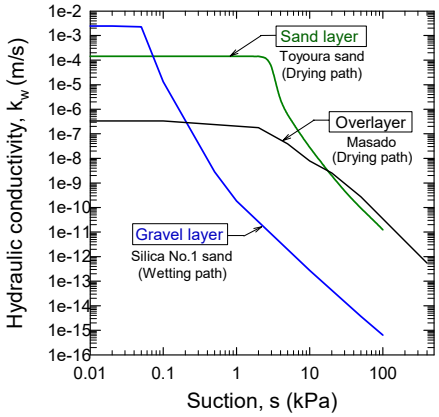

(b) Hydraulic conductivity

Fig. 4 The SWCCs and hydraulic conductivities for sand, gravel, and Masado soils

Table 2 Fitting parameters for the SWCCs

Soil sample	θ_s	AEV	EX	F&X model		
				a	*n*	*m*
Toyoura sand	0.432	2.45	-	2.80	10.02	0.75
Silica sand No.1	0.389	-	0.05	0.39	0.015	0.07
Masado	0.350	2.40	-	6.00	1.19	0.70

Note: θ_s = saturated volumetric water content, AEV = the air entry value (kPa), and EX = the air expulsion value

No. 1 were 1.45×10^{-4} m/s and 2.44×10^{-3} m/s, respectively, it can be understood that the difference (about 17 times) in permeability of the two samples required by the CB system is sufficient.

The soil–water characteristic curves (SWCCs) related to the infiltration behavior for unsaturated soil were estimated using the fitting equation (i.e., Eqs. (1) and (2)) proposed by Fredlund and Xing (1994). Fig. 4(a) shows the SWCCs for sand, gravel, and Masado soils. The fitting parameters of the SWCCs are summarized in Table 2. An AEV of 2.30 kPa and an air expulsion value of 0.05 kPa were derived for Toyoura sand and silica sand No. 1, respectively. As shown in Fig. 4(a), it was observed that there is a difference in the suction value for the VWC between the two soils. As previously mentioned for the CB system, these different suction values indicate that the soils have distinct water

retention capacities of the water that infiltrates the sand layer (Morel-Seytoux 1993, Morris and Stormont 1999, Aubertin 2009). Notably, the SWCC parameters in the L_D estimation equation (i.e., Eq. (3)) proposed by Steenhuis *et al*. (1991) were also set considering the sand layer (drainage process or drying path) and gravel layer (absorption process or wetting path). The drainage process (i.e., drying path) and absorption (i.e., wetting path) process conditions in this study were set for the sand and gravel layers, respectively, because the processes of drainage of the infiltration water from the sand layer and its absorption into the gravel layer in the CB system determine the water-shielding performance of the system.

$$\theta = C(\psi)\left\{\frac{\theta_s}{\ln[e+(\psi/a)^n]}\right\}^m \quad (1)$$

where ψ = the total soil suction; e = the natural logarithmic constant (2.71828); a = a soil parameter related to the air-entry value (AEV) of the soil (kPa); n = a soil parameter that controls the slope at the inflection point in the soil–water retention curve; m = a soil parameter related to the residual water content of the soil; and $C(\psi)$ = the correction function for the soil–water retention curve at the suction of 1,000,000 kPa and zero water content, defined as

$$C(\psi) = \left[1 - \frac{\ln(1+\psi/\psi_r)}{\ln(1+10^6/\psi_r)}\right] \quad (2)$$

$$L_D = \tan\Phi \cdot \{\frac{1}{b}(\frac{1}{\kappa}-1) + \frac{1}{\kappa}(h_{ae}-h_{ex})\} \quad (3)$$

where Φ = the slope of the interface; b = a parameter derived from the equation of the unsaturated hydraulic conductivity ($k = k_{sat}\cdot\exp(b\psi_m)$) (where k_{sat} = the saturated hydraulic conductivity; ψ_m = the suction (h, cmH_2O)); κ can be derived from the relationship of $\kappa = q_v/k_{sat}$ (where q_v is the flux of the water entering the soil); h_{ae} = the sand AEV; and h_{ex} = the air expulsion value of gravel.

On the other hand, it is known that the SWCC of unsaturated soils is hysteretic. The effect of the hysteresis of the SWCC corresponding to the drying and wetting paths affects the hydromechanical properties of soil (Zhai *et al*. 2017, 2020). Thus, the water-shielding performance of the CB system changes depending on the hysteresis of the SWCCs under different conditions such as volume change and confining pressure, etc. However, since the water-shielding performance of the CB system is generally estimated based on the main drying path of fine-grained soil and the main wetting path of coarse-grained soil obtained in the laboratory, this study focused on verifying the performance of the CB system based on the main drying and wetting paths without considering the influence of the hysteresis.

The unsaturated permeability coefficients for the sand and gravel layers were estimated using the following equations (i.e., Eqs. (4) and (5)) by Fredlund *et al*. (1994). The obtained values are shown in Fig. 3(b). It is observed that the permeability coefficient of Toyoura sand is larger for the suction value of about 0.07 kPa or more, which is the intersection of the two results. This difference between the two soils can also be understood concerning the CB system's capability of retaining infiltrated water.

Table 3 Conditions of the seepage analysis for the SSCB model test

Case		1	2	3
Sand layer	ρ_{di} (g/cm^3)	1.50	1.50	1.50
	w_i (%)	0.7	0.7	0.7
	θ_i	0.01	0.01	0.01
Gravel layer	ρ_{di} (g/cm^3)	1.64	1.64	1.64
	w_i (%)	1.0	1.0	1.0
	θ_i	0.01	0.01	0.01
Rainfall intensity, I (mm/h)		20	50	100
Slope angle, Φ (°)		10	10	10
Analysis time (h)		6	6	6

Note: ρ_{di} = initial dry density, w_i = initial water content, and θ_i = initial volumetric water content

$$k_r = \Theta^q(\psi)\frac{\int_{\ln(\psi)}^{b}\frac{\theta(e^y)-\theta(\psi)}{e^y}\theta'(e^y)dy}{\int_{\ln(\psi_{aev})}^{b}\frac{\theta(e^y)-\theta_s}{e^y}\theta'(e^y)dy} \quad (4)$$

$$k_w = k_r \cdot k_{sat} \quad (5)$$

where k_r = the relative hydraulic conductivity; $\Theta^q(\psi)$ = a correction factor (1.0); b = a constant of $\ln(10^6)$; θ' = the derivative of Eq. (5); y = a dummy variable of the integration representing; and k_{sat} = the saturated hydraulic conductivity. suction; ψ_{aev} = the AEV of the soil; and θ_s = the saturated VWC.

Because the air-dried water content of silica sand No. 1 used in the CB model test was about 1.0%, the initial suction value of the gravel layer was set as 21 kPa, corresponding to the SWCC. Based on this value, the initial suction value of the sand layer was set.

In Cases 1–3 in the seepage analysis (described later), the rainfall intensity was set as 20, 50, and 100 mm/h (as in the laboratory CB model test), respectively. Because rainfall infiltration was considered to occur on the entire surface of the sand layer, the entire surface of the sand layer was set as a potential seepage boundary. In the SEEP/W (2004) framework, the total rainfall permeated for a small rainfall event, based on the saturation permeability coefficient of the ground layer, was set as the surface runoff for a large rainfall event. The general governing differential equation for two-dimensional seepage is

$$\frac{\partial}{\partial x}\left(k_x\frac{\partial H}{\partial x}\right) + \frac{\partial}{\partial y}\left(k_y\frac{\partial H}{\partial y}\right) + Q = \frac{\partial\theta}{\partial t} \quad (6)$$

where H = the total head; k_x and k_y = the hydraulic conductivities in the x- and y-directions, respectively; Q = the applied boundary flux; θ = the VWC; and t = the time.

Eq. (1) indicates that the difference in the flow (flux) entering and leaving an elemental volume at a certain time point is equal to the change in the storage of the soil systems. This fundamental expression specifies that the sum of the rates of change in the lows in the x- and y-directions and externally applied flux is equal to the rate of change in

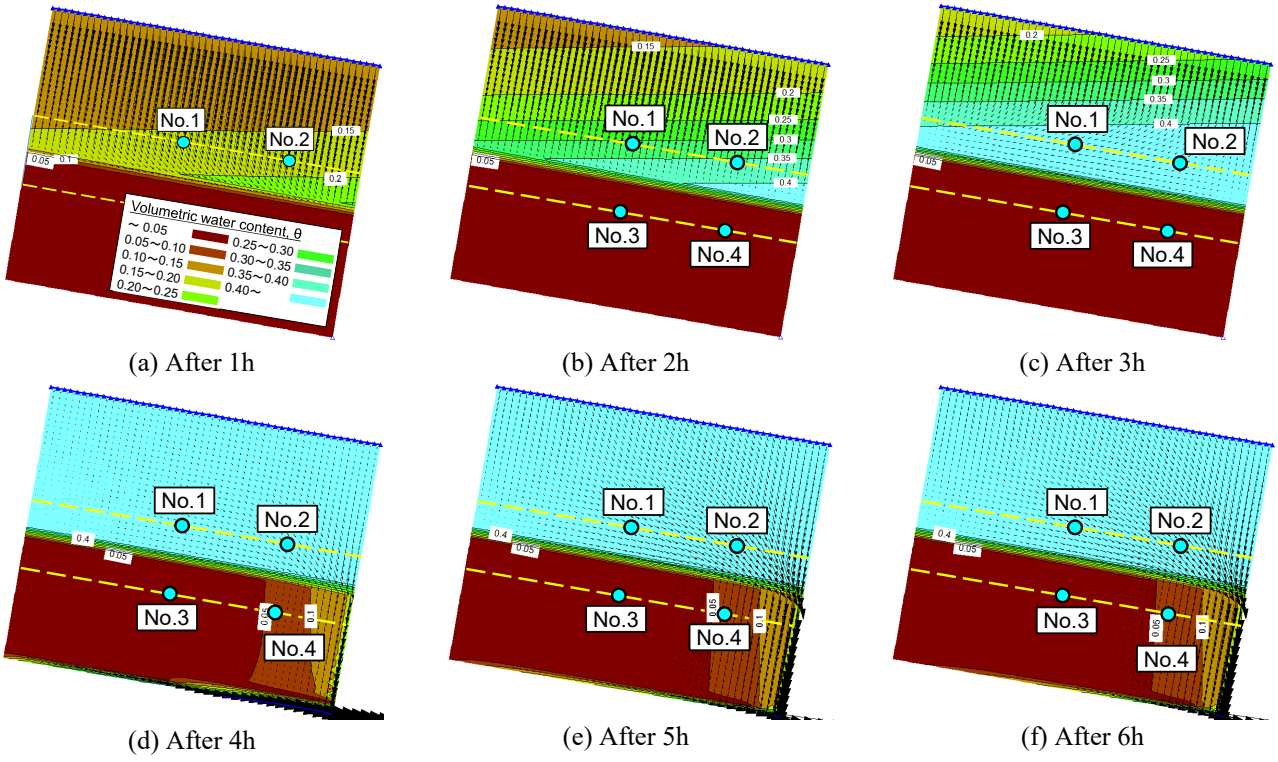

(a) After 1h (b) After 2h (c) After 3h

(d) After 4h (e) After 5h (f) After 6h

Fig. 5 The infiltration behavior for Case 1 (I = 20 mm/h) in the seepage analysis

the VWC with time. In this study, because the largest rainfall intensity of I = 100 mm/h was smaller than that corresponding to the saturation permeability coefficient of the sand layer, 1.45×10^{-2} cm/s (I = 522 mm/h), all of the rainfall was considered to infiltrate the sand layer.

As in the laboratory CB model test, the boundaries between the right and left sides in the analysis model were set to be in a lateral no-flow (i.e., undrained) condition.

These testing conditions reproduced the extreme infiltration condition in which a breakthrough in the CB system occurs due to rainfall infiltration from the surface layer. Thus, in this seepage analysis, only the node (marked by △) at the lower right end of the analysis model with the entire surface of the sand layer was set as the potential seepage boundary. The seepage analysis was performed for 6 h, as in the laboratory CB model test. The conditions of the seepage analysis for the SSCB model test are summarized in Table 3.

2.3 Analysis results and discussion

The four sensors (Nos. 1 and 2 for the sand layer, and Nos. 3 and 4 for the gravel layer) in the seepage analysis were placed in the same positions as those in the model test, as shown in Fig. 1(b). To identify the occurrence of the breakthrough of the CB system at the measurement points, the VWC (θ_{WIH}) in the wetting process of the SWCC for the gravel (silica sand No. 1) was defined as 0.06 based on a water infiltration value (WIH), as shown in Fig. 4(a). Notably, the WIH indicates the reference point at which water rapidly enters the pores of the soil for a given residual VWC of the SWCC.

Figs. 5-7 show the infiltration behaviors after 1, 2, 3, 4, 5, and 6 h in the seepage analysis for Cases 1 under I = 20, 50, and 100 mm/h, respectively. In Case 1 (Fig. 5), the VWCs of the sand layer at measurement points 1 and 2 (i.e., the position of sensor Nos. 1 and 2) increased rapidly after the rainfall. The VWCs for the two points became 0.432 after approximately 3.0 h, indicating the saturation of the sand layer, as shown in Figs. 5(d) and 8(a). In contrast, the VWCs at measurement points 3 and 4 (i.e., the position of sensor Nos. 3 and 4) remained nearly constant until approximately 3.8 h. After 3.8 h, the values at the two points changed simultaneously. Thus, the breakthrough occurred at approximately 3.8 h, and the water-shielding performance of the CB system was maintained until approximately 3.8 h from the start of the rainwater infiltration. According to the VWC distribution for Case 1, as shown in Figs. 5(a)-5(c), the VWCs corresponded to a dry state with θ = 0.06 or lower in the upstream part of the gravel layer. Moreover, the flow vectors indicated that water accumulated at the interface between the sand and gravel layers as a function of the CB. A higher rainfall intensity corresponded to a smaller area in which the VWC was maintained at values lower than θ = 0.06 and a smaller L_D. As in the SSCB model experiment, the right side of the sand layer was set to be in the no-flow (i.e., undrained) condition in the seepage analysis. Therefore, the saturated zone in the sand layer gradually increased if no breakthrough occurred at 3 h, as shown in Figs. 5(a)-5(c).

In Case 2 (I = 50 mm/h, Fig. 6), at measurement points 1 and 2, the VWC of the sand layer increased since the beginning of the rainfall, as in Case 1, and θ became 0.432 at 1.5 h (Fig. 8(a)). Subsequently, the sand layer exhibited a steady state. At measurement point 3 of the gravel layer, the

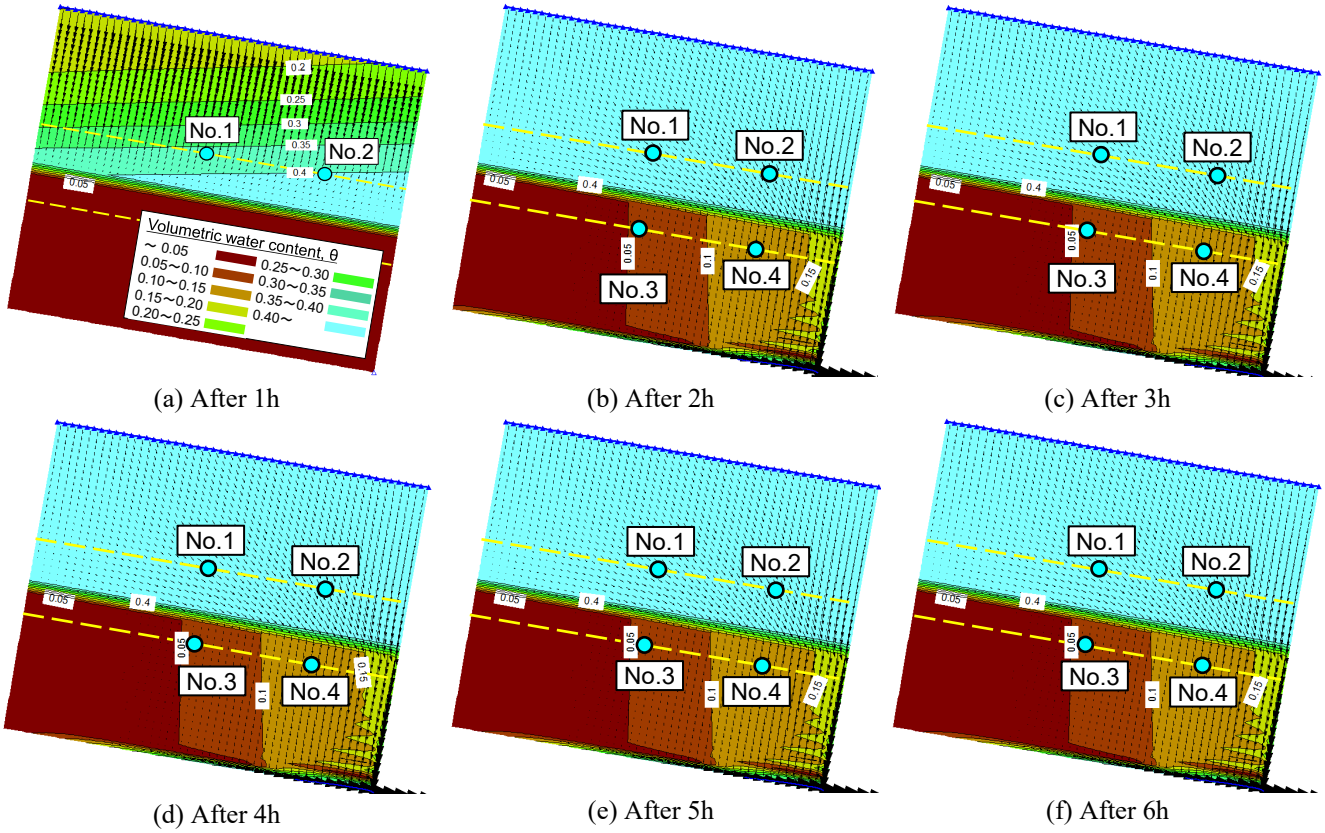

(a) After 1h (b) After 2h (c) After 3h

(d) After 4h (e) After 5h (f) After 6h

Fig. 6 The infiltration behavior for Case 1 (I = 50 mm/h) in the seepage analysis

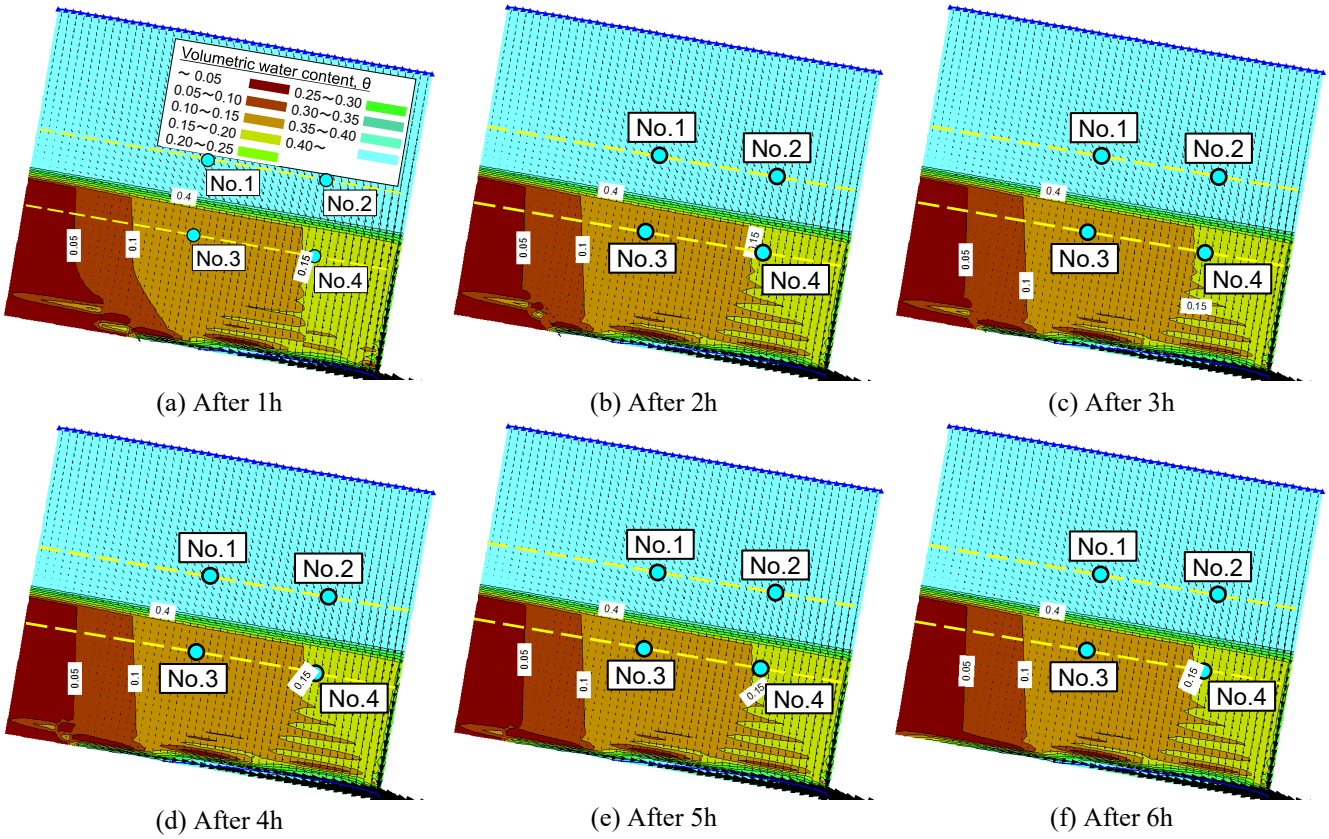

(a) After 1h (b) After 2h (c) After 3h

(d) After 4h (e) After 5h (f) After 6h

Fig. 7 The infiltration behavior for Case 1 (I = 100 mm/h) in the seepage analysis

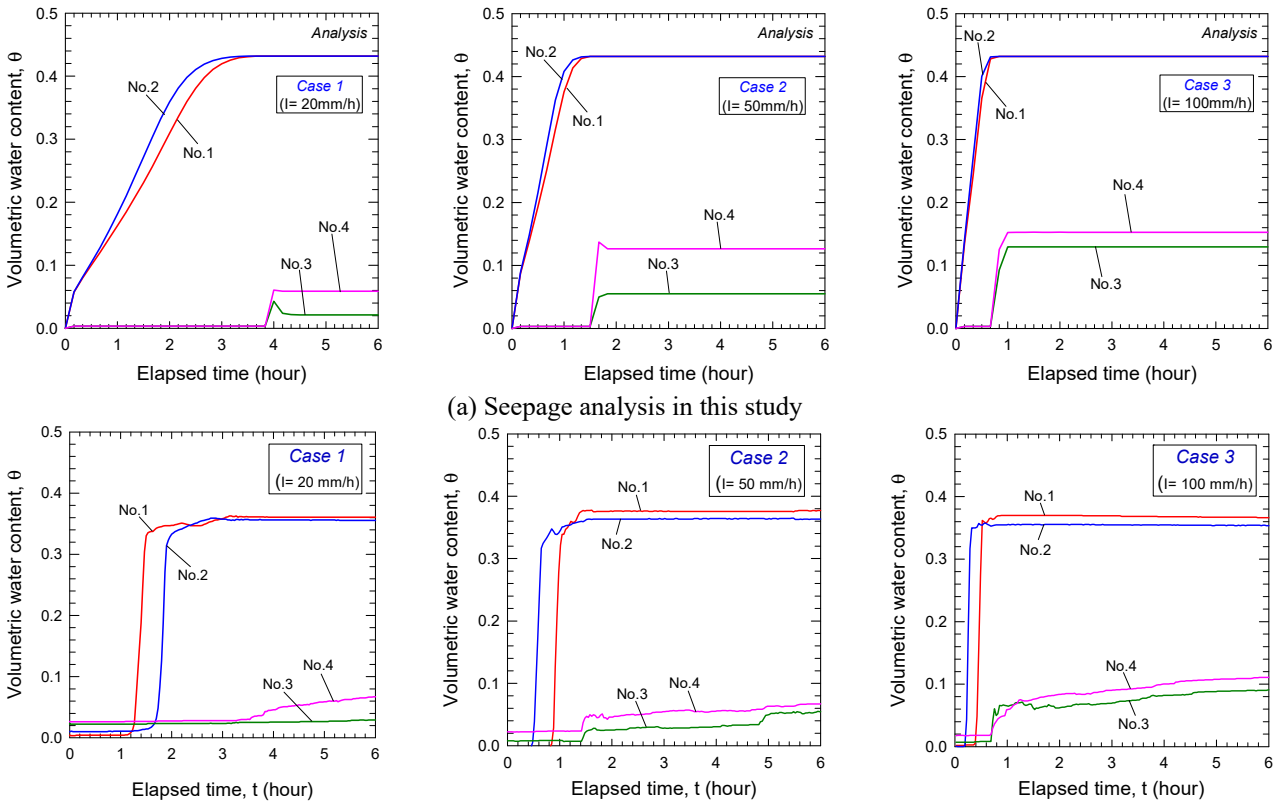

(a) Seepage analysis in this study

(b) The data measured from the SSCB model test by Kim (2021)

Fig. 8 The measurement results of volumetric water contents in the seepage analysis and the SSCB model test

VWC increased from 0.003 to 0.055 after 1.7 h. This tendency was also observed for the VWC shown in Figs. 6(a) and 6(b). Thus, the gravel layer at the measurement point 3 exhibited a steady state, which indicated that the breakthrough occurred at point 3 after 1.7 h. In other words, the CB was maintained at point 3 when the VWC was 0.06 or lower. At measurement point 4, the VWC increased from 0.003 to 0.136 after 1.7 h. Thus, penetration occurred up to point 4 in 1.7 h.

In Case 3 (I = 100 mm/h, Fig. 7), at measurement points 1 and 2, the VWC of the sand layer reached 0.432 after 0.8 h, as in Cases 1 and 2 (Fig. 7(a)). This tendency was also observed through the variation in the VWCs, as shown in Fig. 8(a). Subsequently, the sand layer exhibited a steady state. At measurement point 3, the VWC of the gravel layer increased to 0.093 after 0.8 h and 0.130 after 10 min, thereby reaching a steady state. Thus, the breakthrough occurred 0.8 h after the rainfall. At measurement point 4, the VWC increased to 0.153 at 0.8 h, thereby reaching a steady state.

In all cases, because the VWC did not increase at points 3 and 4 (gravel layer) until the sand layer was saturated, the breakthrough did not occur until the saturation of the sand layer. As summarized in Table 4, breakthrough events occurred 3.8, 1.7, and 0.8 h after the onset of rainfall at rainfall intensities of 20, 50, and 100 mm/h, respectively.

The amount of rainfall associated with the breakthrough occurrence points (BOPs) in each case was similar (80–83 mm). In general, because the total rainfall at which breakthrough occurs is affected by various factors such as

Table 4 Breakthrough occurrence time for each case

Case	I (mm/h)	Breakthrough occurrence time, *t* (h)	
		SSCB	Analysis
1	20	3.8	3.5
2	50	1.7	1.4
3	100	0.8	0.8

the size of the soil tank, sand layer thickness, drainage conditions, rainfall intensity, slope angle, and soil permeability, future work can be focused on examining this value under different parameters. In this study, at points 3 and 4, the infiltration water flowed through the infiltration path without increasing the VWC to a state of saturation because the permeability coefficient of the gravel layer was higher than that associated with the rainfall intensities in each case. In addition, the VWC at point 4 (located downstream) was higher than that at point 3 (located upstream) owing to the influence of gravity on the water-shielding performance of the CB system.

Fig. 8(b) shows the measured VWCs for each case in the SSCB model test conducted by Kim (2021). First, the VWCs at points 1 and 2 in all cases of seepage analysis gradually increased with the rainfall infiltration (Fig. 8(a)), but in the model test, it showed a rapid increase after water infiltrated into the sand layer contacted the sensor (Fig. 8(b)). This difference can be understood that the VWC of the sand layer is taken into account immediately with the onset of rainfall infiltration from the surface layer in the seepage analysis. In the steady state for the water infiltration, the equilibrium state of VWC is observed in all

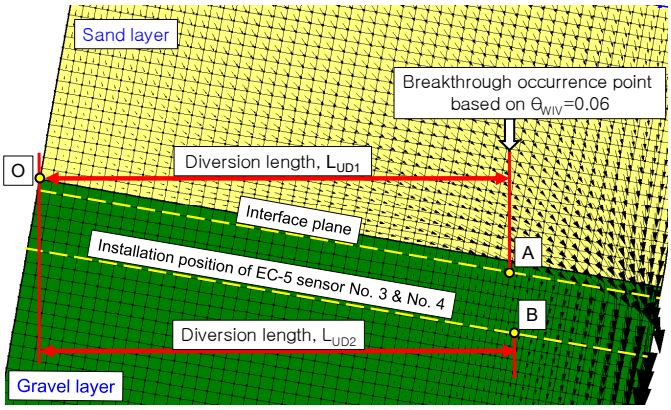

Fig. 9 The criteria for measuring the diversion length in the seepage analysis

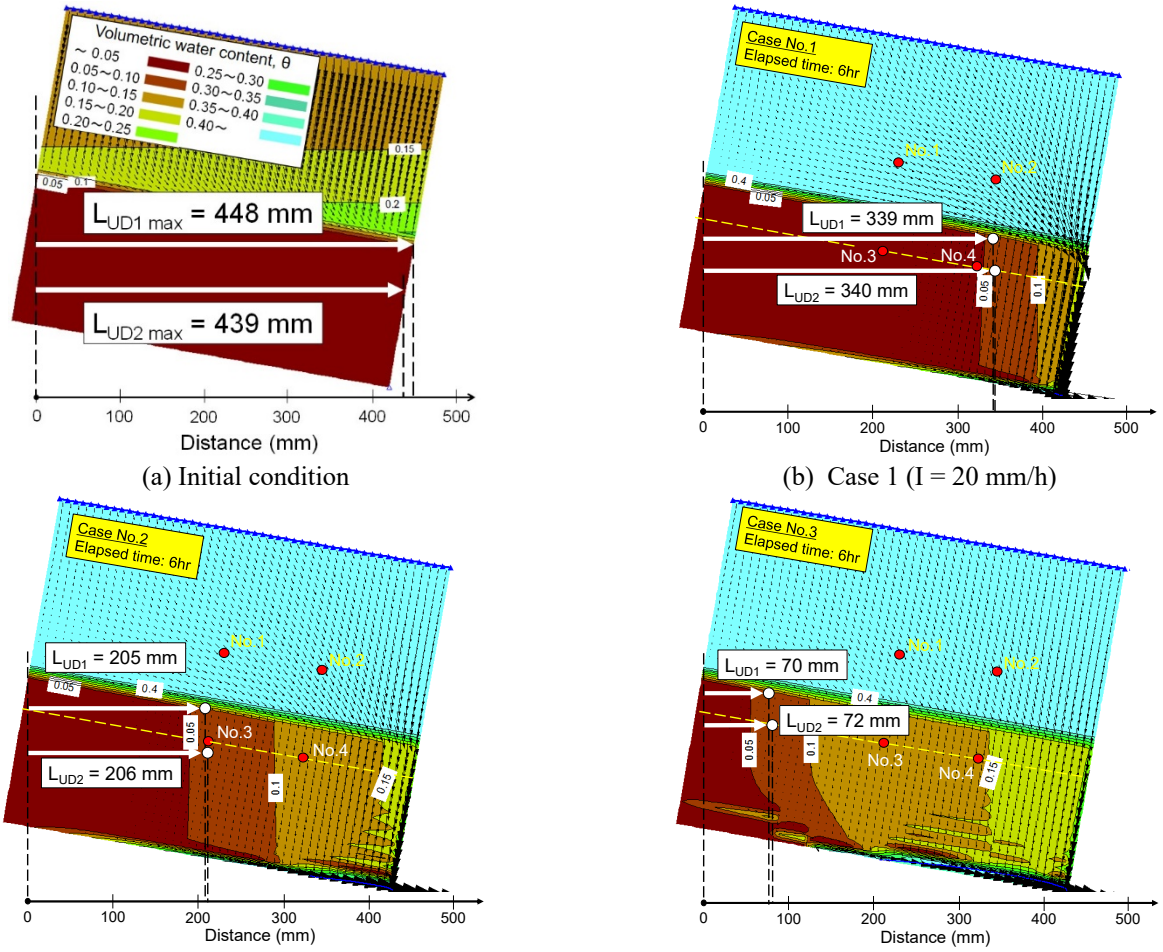

(a) Initial condition

(b) Case 1 (I = 20 mm/h)

(c) Case 2 (I = 50 mm/h)

(d) Case 3 (I = 100 mm/h)

Fig. 10 Measurement results of the diversion lengths for each case in the seepage analysis

sensors in the analysis (Fig. 8(a)), but the equilibrium state at points 3 and 4 of the model test is not constant (Fig. 8(b)). This difference is due to the instability of the area in contact with the EC-5 sensor and the water penetrating through the pores in the soil in the model test. On the other hand, although the VWC values at points 1 and 2 (sand layer) in the model test increased due to rainfall infiltration, they did not become fully saturated (Fig. 8(b)), in contrast to the seepage analysis (Fig. 8(a)) in which complete saturation was observed. This difference likely occurred because the region near the sensor was not completely saturated owing to the presence of an air cavity and the generation of a water path in the soil. Consequently, the VWCs at points 3 and 4 were slightly lower than those estimated in the seepage analysis and exhibited irregular values. Comparing the saturation times of the sand layer in the analysis and model test based on sensor No.2, as the saturation times were 3.4h: 2.9h for Case 1, 1.4h: 1.4h for Case 2, and 0.6h: 0.5h for Case 3 (Figs. 8(a) and 8(b)), respectively, it can be seen that the sand layer in the

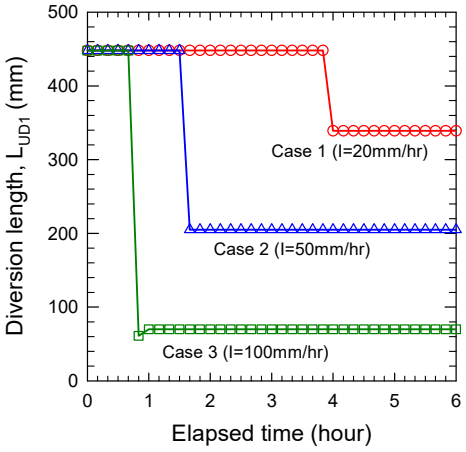

(a) Interface plane between sand and gravel layers

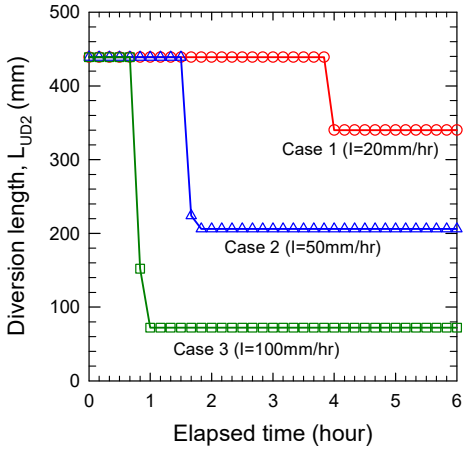

(b) Measurement line of the installation position of EC-5 sensors Nos. 3 & 4

Fig. 11 Variation of the diversion lengths measured in the seepage analysis

analysis and model test was saturated at similar times. The breakthrough occurrence time was determined considering the rapid increase in the VWCs at points 3 and 4 of the gravel layer. As shown in Figs. 8(a) and 8(b), the breakthrough occurrence times associated with the seepage analysis and model test were 3.8 h: 3.5 h (210 min), 1.7 h: 1.4 h (85 min), and 0.8 h: 0.8 h (45 min), respectively. The consistency of the results obtained using the two methods demonstrated the high accuracy of the breakthrough occurrence prediction based on the seepage analysis in this study.

3. Comparison of diversion lengths in the model test and seepage analysis

3.1 Criteria for determining L_D in the seepage analysis

To evaluate the L_D values in the seepage analysis, it was necessary to set the standard point at which the breakthrough occurred. As shown in Fig. 4(a), the VWC (θ_{WIH}) corresponding to the suction value of 0.12 kPa was defined as 0.06 based on the absorption (wetting) curve of the gravel SWCC, similar to the method of determining the residual degree of saturation (S_{r0}) in the SWCC (Fredlund and Xing 1994). Thus, the case in which the VWC of the gravel layer was lower than θ = 0.06 was defined as the condition in which infiltration in the CB system occurred, that is, the breakthrough occurred. The suction value of 0.12 kPa corresponded to a point in the absorption curve at which the water content started to increase rapidly from the residual state. In the SSCB model test, the moisture state of the gravel was observed based on two patterns near the boundary and installation depth of the EC-5 sensors (50 mm below the boundary of the two soil layers, i.e., Nos. 3 and 4 corresponding to the gravel layer), and the diversion lengths L_{UD1} and L_{UD2} (undrained diversion length) were measured.

This configuration was followed because when the breakthrough occurred, the water obliquely and nonlinearly infiltrated the interface between the sand and gravel layers, and the position at which the breakthrough occurred was challenging to determine. Thus, as in the SSCB model test, the CB performance in the analysis was evaluated based on the two patterns. First, as shown in Fig. 9, the horizontal distance from the most upstream node (point O) of the interface between the sand and gravel layers to point A (BOP), at which the VWC was lower than θ = 0.06, was defined as L_{UD1}. The horizontal distance from point O to point B, corresponding to the measurement line of the EC-5 sensors in the SSCB model test, was defined as L_{UD2}.

Table 5 Diversion lengths derived from the SSCB model test and the seepage analysis

Case	I (mm/h)	L_{UD1} (cm)		L_{UD2} (cm)	
		SSCB	Analysis	SSCB	Analysis
1	20	13.5	33.9	24.8	34.0
2	50	11.7	20.5	11.2	20.6
3	100	0	7.0	0	7.2

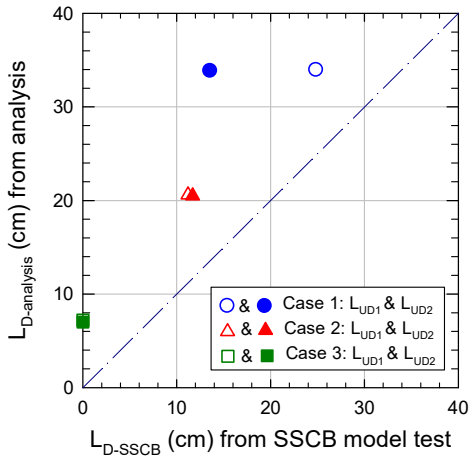

Fig. 12 Comparison of diversion lengths between the seepage analysis and the SSCB model test

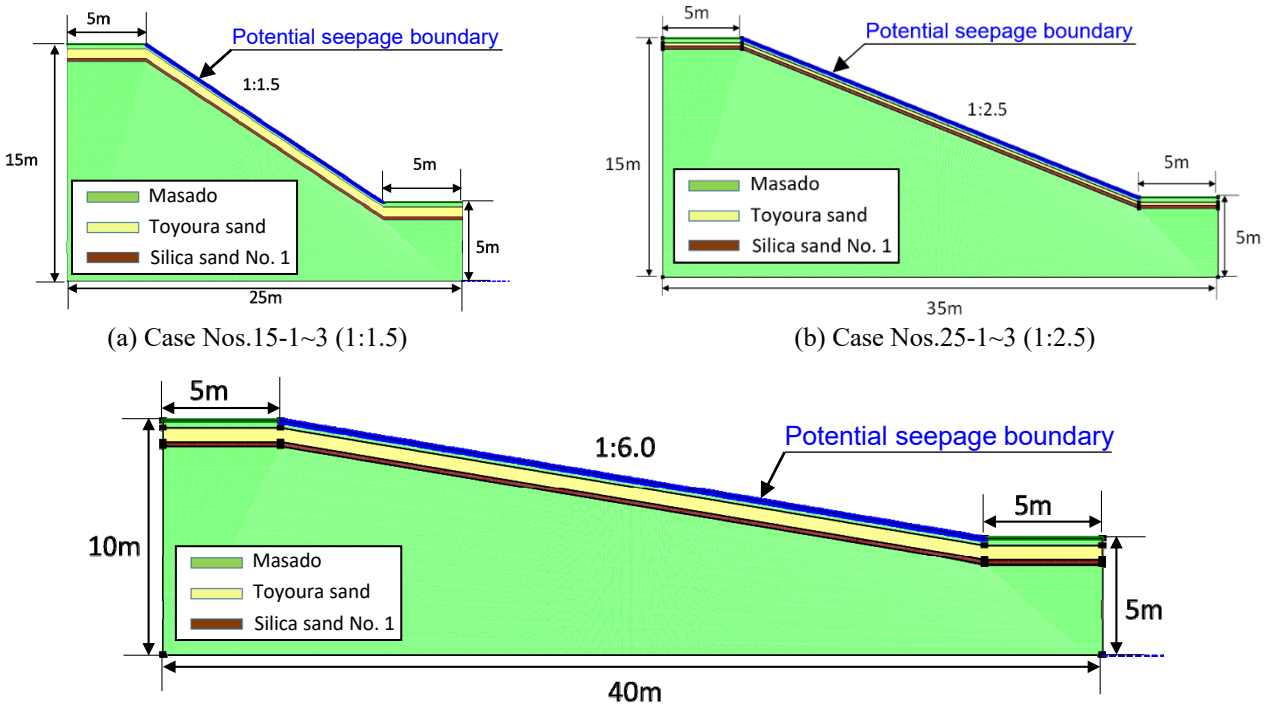

(a) Case Nos.15-1~3 (1:1.5)

(b) Case Nos.25-1~3 (1:2.5)

(c) Case Nos.60-1~3 (1:6.0)

Fig. 13 Variation of the diversion lengths measured in the seepage analysis

Table 6 Diversion lengths derived from the seepage analysis for the engineered slopes

Case	Slope angle	Layer thickness (cm)			I (mm/h)	$L_{D\text{-slope-analysis}}$ (cm)
		Overlayer	Sand layer	Gravel layer		
No.15-1	1:1.5 (33.7°)	30	20	20	20	199.7
No.15-2			40			291.2
No.15-3			60			316.1
No.25-1	1:2.5 (21.8°)	30	20	20	20	157.8
No.25-2			40			232.1
No.25-3			60			255.3
No.60-1	1:6.0 (9.5°)	30	20	20	20	108.5
No.60-2			40			143.0
No.60-3			60			152.9

3.2 Comparative evaluation of the LD values

Figs.10(a)-10(d) show the measured L_D after 6 h for each case in the seepage analysis. As shown in Fig. 8(a), the L_D values in the case in which breakthrough did not occur in the initial condition of seepage analysis were $L_{UD1\text{-}max}$ = 448 mm (interface plane between the two layers) and $L_{UD2\text{-}max}$ = 439 mm (measurement line of the EC-5 sensor). The numbers in Fig. 10 represent the VWC. As in the SSCB model experiment conducted by Kim (2021), the infiltration behavior was observed for 6 h in the seepage analysis. As described in Section 2.3, in this study, the BOP was determined based on the VWC of θ = 0.06, and the L_D values for the different cases were as follows: Case 1 (20 mm/h): L_{UD1} = 339 mm, L_{UD2} = 340 mm; Case 2 (50 mm/h): L_{UD1} = 205 mm, L_{UD2} = 206 mm; Case 3 (100 mm/h): L_{UD1} = 70 mm, L_{UD2} = 72 mm. In the seepage analysis, the two diversion lengths were similar in the depth direction because the infiltration in the gravel layer occurred in the vertical direction. The width of the mesh near the interface between the sand and gravel layers in this analysis was finely divided by 8.0 to 9.0 mm to eliminate its influence on the limit length. Table 5 summarizes the L_D values measured in the seepage analysis, and Fig. 11 shows the variation in the measured L_D. After the breakthrough, the steady state was maintained, and the L_D values did not vary. This tendency in the seepage analysis was similar to the infiltration behavior observed in the laboratory SSCB model test conducted by Kim (2021).

Fig. 12 shows the comparison of the L_D values obtained in the seepage analysis and SSCB model test conducted by Kim (2021). In the figure, the symbols ○ and ● for Case 1 (20 mm/h), △ & ▲ for Case 2 (50 mm/h), and □ & ■ for Case 3 (100 mm/h) indicate L_{UD1} and L_{UD2}, respectively.

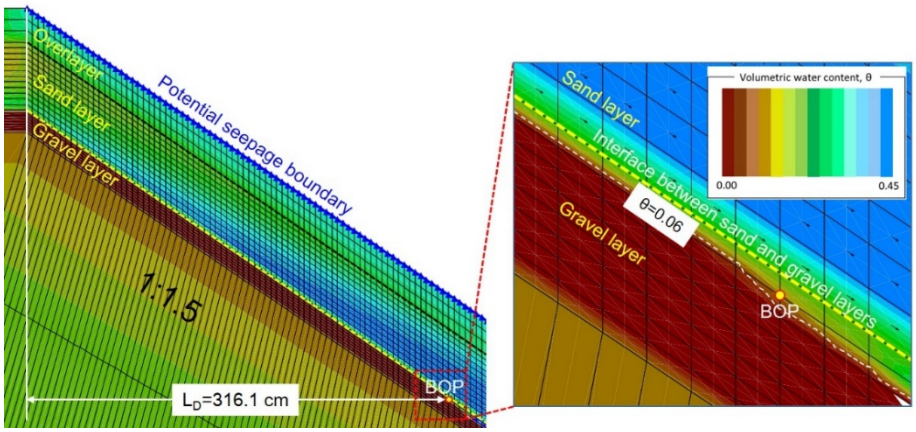

(a) Case No.15-3

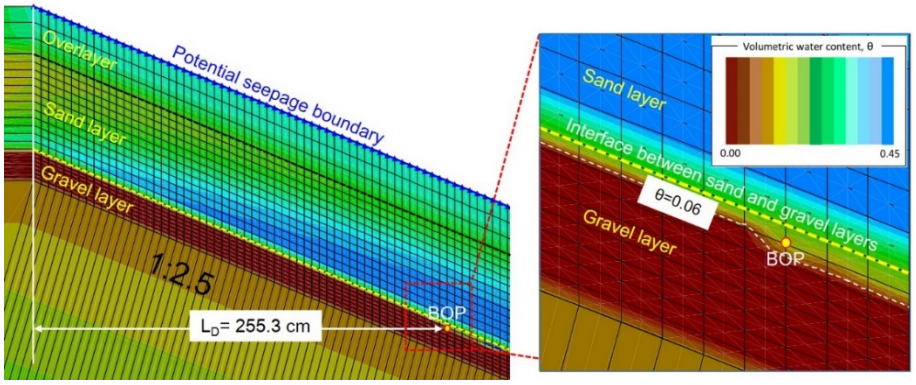

(b) Case No. 25-3

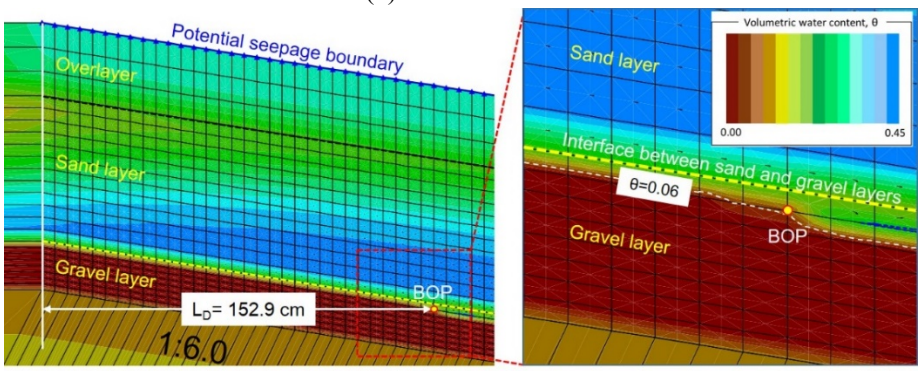

(c) Case No. 60-3

Fig. 14 Measurement of the diversion length according to the slope angles (sand layer thickness = 60 cm)

Compared with the values presented in Table 5, the diversion lengths ($L_{D\text{-analysis}}$) obtained in the seepage analysis were slightly larger than those ($L_{D\text{-SSCB}}$) obtained in the SSCB model test. The maximum difference in the values estimated using the two methods corresponded to L_{UD2} in Case 1. In other words, the seepage analysis slightly overestimated the water-shielding performance of the CB system. This finding was expected because the criterion for determining the BOP in the seepage analysis was defined as $\theta_{WIH} = 0.06$, as shown in Fig. 4(a). The difference between the two results can be decreased by setting the criterion of the VWC (θ_{WIH}) at the point at which breakthrough occurs to be lower than 0.06. Considering the differences between the two results, the criteria for the breakthrough occurrence must be further discussed. The results obtained in this study indicated that the relationship of L_{UD2} based on the measurement line of the EC-5 sensor was more reasonable than that of L_{UD1} based on the interface plane between two layers.

4. Analytical verification of the CB system of the engineered slope

In this study, the infiltration characteristics of the engineered slopes at different slope angles and sand layer thickness values, which considerably influence the water-shielding performance of the CB system, are investigated

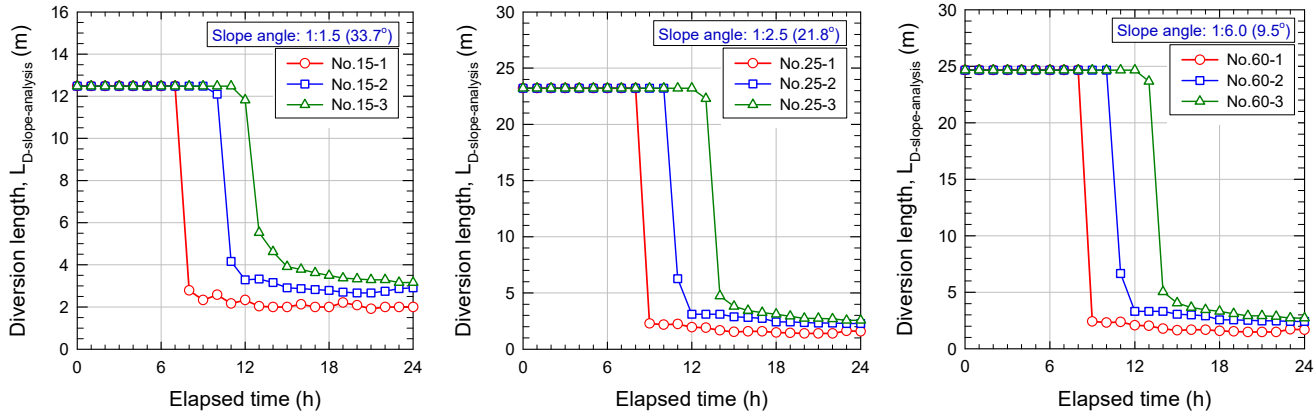

(a) Case Nos.15-1~3 (b) Case Nos.25-1~3 (a) Case Nos.60-1~3

Fig. 15 Variation of the diversion lengths for Case No.15 of 1:1.5 (33.7°), Case No.25 of 1:2.5 (21.8 °), and Case No.60 of 1:6.0 (9.5 °) for 24 h

by a series of seepage analyses using SEEP/W (2004). The L_D values obtained using the seepage analysis were compared with those of the laboratory SSCB model test conducted by Kim (2021).

4.1 Seepage analysis model and conditions

To investigate the infiltration characteristics of the CB system at the in situ slope, a series of seepage analyses were performed with different sand layer thickness values (20, 40, and 60 cm) and slope angles (i.e., Case 15 with 1:1.5 (33.7°), Case 25 with 1:2.5 (21.8°), and Case 60 with 1:6.0 (9.5°)) were performed. The conditions are presented in Table 6. As shown in Fig. 13, the analysis models for the three cases were established according to the slope angle ratios based on a width of 5.0 m at the top and bottom of the slope and a depth of 5.0 cm at the bottom of the slope. The overlayer thickness was 30 cm, the gravel layer thickness was 20 cm, and the rainfall intensity was 20 mm/h. The element sizes in the overlayer and sand layer were set as 10.0×5.0 cm (width × height), and 5.0×5.0 cm, respectively. The element size for the gravel layer was set as 2.5×5.0 cm, denser than the other layers, to determine the L_D based on the changes in the VWC.

The saturation permeability coefficients of the sand and gravel layers were set considering those of Toyoura sand (k_{sat}= 1.45×10^{-4} m/s) and silica sand No. 1 (k_{sat}= 2.44×10^{-3} m/s), as in the laboratory SSCB model test conducted by Kim (2021). The saturation permeability coefficient of decomposed granite soil (i.e., Masado) for ρ_d =1.64 g/cm^3 was set as 3.34×10^{-6} m/s. The SWCCs of the three types of soils are shown in Fig. 4(a). The drying (drainage) process of the SWCC for the overlayer and sand layer was considered, and the wetting (absorption) process of the SWCC for the gravel layer was considered. Because the air-dried water content of silica sand No. 1 used in the CB model test was 1.0%, the initial suction value of the gravel layer was set as 21 kPa corresponding to the SWCC, and based on this value, the initial suction values for each layer were automatically set in the SEEP/W program, as in the previous analysis for the laboratory SSCB model test. The input parameters of SWCCs for the seepage analysis are summarized in Table 2. All the seepage analyses were performed for 24 h to evaluate the infiltration characteristics in the steady state during rainfall.

4.2 Analysis results and discussion

The occurrence of the breakthrough in the CB system of the engineered slope was determined based on the VWC of 0.06, as in the previous analysis for the laboratory SSCB model test. L_D was defined as the horizontal distance from the starting point of the top of the slope to the breakthrough point. Fig. 14 shows the L_D values for Cases 15, 25, and 60 for the sand layer of 60 cm (1:6.0) after 24 h. In the figures, the dotted line indicates the VWC (θ_{WIH}) of 0.06 in the ground. The points at which the VWC changes to 0.06 can be observed at the interface between the sand and gravel layers by magnifying the vicinity of the BOP. The following L_D values were obtained from the seepage analysis for the engineered slopes, as indicated in Table 6: Case 15-1–3: 240, 350, and 380 cm, respectively; Case 25-1–3: 170, 250, and 275 cm, respectively; and Case 60-1–3: 110, 145, and 150 cm, respectively.

Fig. 15 shows the L_D variations in Cases 15, 25, and 60 in 24 h. The infiltration states for each case exhibited a steady state after 24 h. When the sand layer thickness was 20, 40, and 60 cm, the L_D values decreased sharply after 9 h (Cases 15-1, 25-1, and 60-1), 12 h (Cases 15-1, 25-1, and 60-1), and 14 h (Cases 15-1, 25-1, and 60-1), respectively. A thicker sand layer corresponded to a slower breakthrough occurrence, which indicated that the sand layer thickness influences the time at which the breakthrough occurs. Fig. 16 shows the L_D values corresponding to different sand layer thicknesses and slope angles. The L_D increased as the slope became steeper. In addition, the rate of increase of L_D with the increase in the sand layer thickness from 20 to 40 cm: (Case 15-1→15-2: 46%, 25-1→25-2: 47%, and 60-1→60-2: 32%) were larger than those with the increase in the sand layer thickness from 40 to 60 cm: (Case 15-2→15-3: 9%, 25-2→25-3: 10%, and 60-2→60-3: 7%). Thus, the L_D did not increase continuously with increasing sand layer thickness. These findings indicated that the sand layer

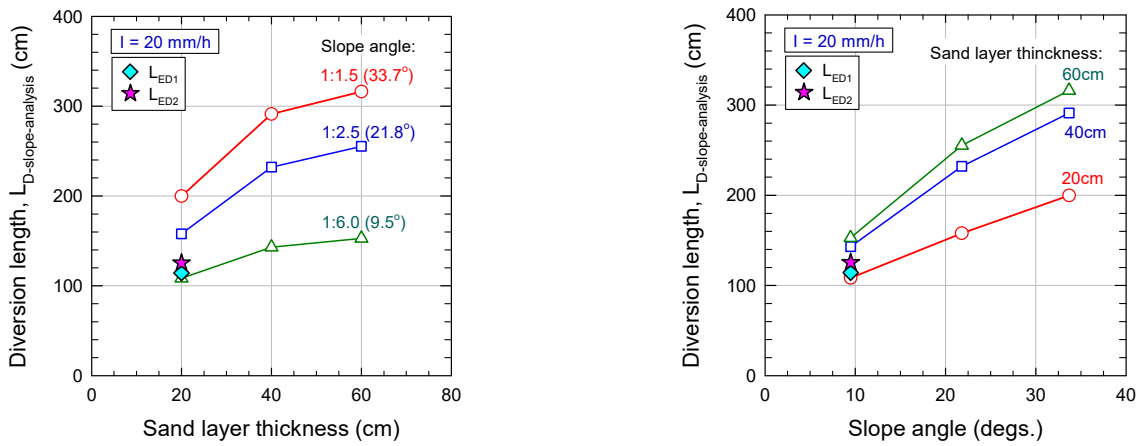

(a) Sand layer thickness vs. $L_{D\text{-slope-analysis}}$ (b) Slope angle vs. $L_{D\text{-slope-analysis}}$

Fig. 16 Variation of diversion lengths according to the sand layer thickness and slope angle

thickness of 40 cm corresponded to the most effective CB system. Therefore, the sand layer thickness of the CB system at a real in situ slope must be efficiently determined through preliminary investigations.

On the other hand, Kim (2021) identified L_{ED1} and L_{ED2} through the laboratory SSCB model test in the lateral no-flow condition to realize the slope design of geo-structures based on the CB system, as explained previously. The following conditions were set for the laboratory SSCB model test: The thicknesses of the sand and gravel layers were 20 cm, the rainfall intensity was 20 mm/h, and the slope angle was 10°. This testing condition was identical to that of Case 60-1 in this study, except for the absence of the overlayer. The diversion lengths (L_{ED1} of 114.2 cm and L_{ED2} of 125.5 cm) estimated by Kim (2021) are shown in Fig. 16. Here, L_{ED1} represents the diversion length in the SSCB model test after the penetration reached the interface between the sand and gravel layers, and L_{ED2} represents the diversion length in the CB model test after the penetration reached the sensor installation level in the gravel layer. As shown in Fig. 16, the values estimated by Kim (2021) were consistent with the L_D of 108.5 cm obtained in the seepage analysis for the engineered slope of Case 60. Thus, the laboratory SSCB model test was validated by the results of the seepage analysis. These findings highlight that the SSCB model proposed by Kim (2021) is a promising alternative for the laboratory CB model test to efficiently evaluate the water-shielding performance of the CB system for an engineered slope.

5. Conclusions

Numerical analyses on the SSCB model test and engineered slopes under the same and additional conditions in this study were carried out to efficiently evaluate the water-shielding performance of the CB system for the stability of the geo-structure. First, to back-analyze the model test in the same conditions as those of the laboratory SSCB model test under the lateral no-flow condition, a series of seepage analyses were performed under three rainfall intensities. Moreover, the infiltration characteristics of the engineered slopes at different slope angles and sand layer thicknesses in the CB system were investigated by a series of seepage analyses. The following conclusions were derived.

(1) According to the seepage analysis results on the SSCB model test, the breakthrough occurred at 3.8, 1.7, and 0.8 h for each case (i.e., I = 20, 50, and 100 mm/h). The amount of rainfall associated with the BOPs in each case was approximately 80 mm. The breakthrough occurrence times in the seepage analysis and model test were similar (i.e., 3.8 h: 3.5 h, 1.7 h: 1.4 h, and 0.8 h: 0.8 h). On the other hand, The L_D values in the seepage analysis based on the VWC (θ_{WIH}) of 0.06 (i.e., indicated the breakthrough occurrence) were slightly larger than those obtained in the model test. The difference between the two results could be alleviated by setting the criterion of the VWC (θ_{WIH}) corresponding to the BOP to be lower than 0.06. The relationship of L_{UD2} based on the measurement line of the EC-5 sensor was more reasonable than that of L_{UD1} based on the interface plane between two layers.

(2) In the seepage analyses of the CB system for the engineered slopes with different sand layer thicknesses and slope angles, a thicker sand layer corresponded to a slower breakthrough occurrence and a larger increase in the L_D. However, the increase rate of L_D with the sand layer thickness exhibited an upper limit. Moreover, the L_D increased as the slope became steeper. According to the findings, the sand layer thickness of 40 cm was expected to correspond to the most effective CB system. On the other hand, the result of L_D=108.5 cm for Case No. 60-1 (slope angle: 9.5°, and sand layer: 20 cm) in the seepage analysis of the CB system for the engineered slopes was agreed well with those (i.e., L_{ED1}=114.2 cm, and L_{ED2}=125.5 cm) from the laboratory SSCB model test by Kim (2021).

(3) From the above results, it can be concluded that the results of the seepage analysis on the SSCB model test and engineered slopes conducted in this study verified the validity of the laboratory SSCB model test. The findings highlight that the experimental methodology of

the SSCB model represents a promising alternative for the laboratory CB model test to efficiently evaluate the water-shielding performance of the CB system for an engineered slope.

Acknowledgments

The present research was supported by the research fund of Dankook University in 2022.

References

Aubertin, M., Cifuentes, E., Apithy, S.A., Bussière, B., Molson, J. and Chapuis, R.P. (2009), "Analyses of water diversion along inclined covers with capillary barrier effects", *Can. Geotech. J.*, **46**(10), 1146-1164. https://doi.org/10.1139/T09-050.

Benson, C.H. and Khire, M.V. (1995), "Earthern covers for semiarid and arid environments", Landfill closures. *Geotech. Spec. Pub.*, **53**, 201-217.

Bussière, B., Aubertin, M. and Chapuis, R.P. (2002), "A laboratory set up to evaluate the hydraulic behavior of inclined capillary barriers", *Proceedings of the international conference on physical modelling in geotechnics*, St. John's, Nfld., Canada, 10-12 July 2002.

Bussière, B., Aubertin, M. and Chapuis, R.P. (2003), "The behavior of inclined covers used as oxygen barriers", *Can. Geotech. J.*, **40**(3), 512-535. https://doi.org/10.1139/t03-001.

Deng, D., Lu, K. and Li, L. (2019), "LE analysis on unsaturated slope stability with introduction of nonlinearity of soil strength", *Geomech. Eng.*, **19**(2), 179-191. https://doi.org/10.12989/gae.2019.19.2.179.

Fredlund, D.G. and Xing, A. (1994), "Equations for the soil-water characteristic curve", *Can. Geotech. J.*, **31**(4), 521-532. https://doi.org/10.1139/t94-061.

Fredlund, D.G., Xing, A. and Huang, S. (1994), "Predicting the permeability function for unsaturated soils using the soil-water characteristic curve", *Can. Geotech. J.*, **31**(4), 533-546. https://doi.org/10.1139/t94-062.

GEO-SLOPE International Ltd. (2004), *Computer Program SEEP/W for Finite Element Seepage Analysis*, User's Guide, Calary, Alta, Canada.

Hey, C. and Simms, P. (2021), "Preliminary assessment of biosolids in covers with capillary barrier effects", *Eng. Geol.*, **280**, 105973. https://doi.org/10.1016/j.enggeo.2020.105973.

Hill, D.E. and Parlange, J.Y. (1972), "Wetting front instability in layered soils", *Soil Sci. Soc. Am. J.*, **36**(5), 697-702. https://doi.org/10.2136/sssaj1972.03615995003600050010x.

Kämpf, M. and Montenegro, H. (1997), "On the performance of capillary barriers as landfill cover", *Hydrol. Earth Syst. Sci.*, **1**(4), 925-930. https://doi.org/10.5194/hess-1-925-1997.

Khire, M.V., Benson, C.H. and Bosscher, P.J. (2000), "Capillary barriers: Design variables and water balance", *J. Geotech. Geoenviron. Eng.*, **126**(8), 695-708. https://doi.org/10.1061/(ASCE)1090-0241(2000)126:8(695).

Kim, B.S. (2021), "Evaluation of the water shielding performance of a capillary barrier system through a small-scale model test", *Appl. Sci.-Basel*, **11**(11), 5231. https://doi.org/10.3390/app11115231.

Kim, Y. and Jeong, S. (2017), "Modeling of shallow landslides in an unsaturated soil slope using a coupled model", *Geomech. Eng.*, **13**(2), 353-370. https://doi.org/10.12989/gae.2017.13.2.353.

Kung, K.J.S. (1990), "Preferential flow in a sandy vadose soil: 2. Mechanism and implications", *Geoderma*, **46**(1-3), 59-71. https://doi.org/10.1016/0016-7061(90)90007-V.

Li, Y., Satyanaga, A. and Rahardjo, H. (2021), "Characteristics of unsaturated soil slope covered with capillary barrier system and deep-rooted grass under different rainfall patterns", *Int. Soil Water Conserv. Res.*, **9**(3), 405-418. https://doi.org/10.1016/j.iswcr.2021.03.004.

Mancarella, D., Doglioni, A. and Simeone, V. (2012), "On capillary barrier effects and debris slide triggering in unsaturated layered covers", *Eng. Geol.*, **147**, 14-27. https://doi.org/10.1016/j.enggeo.2012.07.003.

Matsumoto, K., Kobayashi, K., Morii, T. and Nakajusa, S. (2016), "Evaluation of diversion length of the capillary barrier with nonflatness of regular sine wave shape between sand and gravel layers", *Jpn. Geotech. J.*, **11**(2), 305-313. (In Japanese) https://doi.org/10.3208/jgs.11.139.

Miyazaki, T. (1988), "Water flow in unsaturated soil in layered slopes", *J. Hydrol.*, **102**(1-4), 201-214.

Mohamed, A.M., Shooshpasha, I. and Ong, R.N. (1997), "Diffusion of metal ions in frozen capillary barriers", *Eng. Geol.*, **47**(1-2), 1-15. https://doi.org/10.1016/0022-1694(88)90098-4.

Morel-Seytoux, H.J. (1993), "Dynamic perspective on the capillary barrier effect at the interface of an upper fine layer with a lower coarse layer", *Proceedings of the Engineering Hydrology*, ASCE: Reston, VA, USA.

Morris, C.E. and Stormont, J.C. (1998), "Evaluation of numerical simulations of capillary barrier field tests", *Geotech. Geol. Eng.*, **16**(3), 201-213. https://doi.org/10.1023/A:1008853710339.

Ng, C.W., Liu, J., Chen, R. and Xu, J. (2014), "Physical and numerical modeling of an inclined three-layer (silt/gravelly sand/clay) capillary barrier cover system under extreme rainfall", *Waste Manage.*, **38**, 210-221. https://doi.org/10.1016/j.wasman.2014.12.013.

Nicholson, R.V., Gillham, R.W., Cherry, J.A. and Reardon, E.J. (1989), "Reduction of acid generation in mine tailings through the use of moisture-retaining cover layers as oxygen barriers", *Can. Geotech. J.*, **26**(1), 1-8. https://doi.org/10.1139/t89-001.

Oldenburg, C.M. and Pruess, K. (1993), "On numerical modeling of capillary barriers", *Water Resour. Res.*, **29**(4), 1045-1056. https://doi.org/10.1029/92WR02875.

Parent, S.É. and Cabral, A. (2006), "Design of inclined covers with capillary barrier effect", *Geotech. Geol. Eng.*, **24**(3), 689-710. https://doi.org/10.1007/s10706-005-3229-9.

Rahardjo, H., Santoso, V.A., Leong, E.C., Ng, Y.S. and Hua, C.J. (2011), "Numerical analyses and monitoring performance of residual soil slopes", *Soils Found.*, **51**(3), 471-482. https://doi.org/10.3208/sandf.51.471.

Rasmuson, A. and Eriksson, J.C. (1986), "Capillary barriers in covers for mine waste dumps", *National Swedish Environmental Protection Board*, 3307.

Ross, B. (1990), "The diversion capacity of capillary barriers", *Water Resour. Res.*, **26**(10), 2625-2629. https://doi.org/10.1029/WR026i010p02625.

Satyanaga, A., Moon, S.W. and Kim, J.R. (2022). "Stability analyses of dual porosity soil slope", *Geomech. Eng.*, **28**(1), 77-87. https://doi.org/10.12989/gae.2022.28.1.077.

Steenhuis, T.S., Parlange, J.Y. and Kung, K.S. (1991), "Comment on 'The diversion capacity of capillary barriers' by Benjamin Ross", *Water Resour. Res.*, **27**(8), 2155-2156. https://doi.org/10.1029/91WR01366.

Tami, D., Rahardjo, H., Leong, E.C. and Fredlund, D.G. (2004), "A physical model of sloping capillary barriers", *Geotech. Test. J.*, **27**(2), 11-27. https://hdl.handle.net/10356/101480.

Tang, J., Taro, U., Huang, D., Xie, J. and Tao, S. (2020), "Physical Model Experiments on Water Infiltration and Failure Modes in Multi-Layered Slopes under Heavy Rainfall", *Appl. Sci.-Basel*, **10**(10), 3458. https://doi.org/10.3390/app10103458.

Walter, M.T., Kim, J.S., Steenhuis, T.S., Parlange, J.Y., Heilig, A., Braddock, R.D., Selker, J.S. and Boll, J. (2000), "Funneled flow mechanisms in a sloping layered soil: Laboratory investigation", *Water Resour. Res.*, **36**(4), 841-849. https://doi.org/10.1029/1999WR900328.

Warrick, A.W., Wierenga, P.J. and Pan, L. (1997), "Downward water flow through sloping layers in the vadose zone: Analytical solutions for diversions". *J. Hydrol.*, **192**, 321-337. https://doi:10.1016/S0022-1694(96)03080-6.

Zhan, T.L., Li, H., Jia, G.W., Chen, Y.M. and Fredlund, D.G. (2014), "Physical and numerical study of lateral diversion by three-layer inclined capillary barrier covers under humid climatic conditions", *Can. Geotech. J.*, **51**(12), 1438-1448. https://doi.org/10.1139/cgj-2013-0449.

Zhai, Q., Rahardjo, H. and Satyanaga, A. (2017), "Uncertainty in the estimation of hysteresis of soil–water characteristic curve", *Environ. Geotech.*, **6**(4), 204-213. https://doi.org/10.1680/jenge.17.00008.

Zhai, Q., Rahardjo, H., Satyanaga, A., Dai, G. and Du, Y. (2020), "Estimation of the wetting scanning curves for sandy soils", *Eng. Geol.*, **272**, 105635. https://doi.org/10.1016/j.enggeo.2020.105635.

IC